ORIGINAL RESEARCH

Exploring and Validating the Mechanism of Ulinastatin in the Treatment of Sepsis-Associated Encephalopathy Based on Transcriptome Sequencing

Wen Hu [iD] [1,]*, Xiaoyuan Zhang[1,]*, Zhen Wu[1,]*, Yushan Luo[1,]*, Bailong Hu [iD] [2], Xiaohua Zou [iD] [2]

[1]Guizhou Medical University, Guiyang, Guizhou, 550004, People's Republic of China; [2]Department of Anesthesiology, The Affiliated Hospital of Guizhou Medical University, Guiyang, Guizhou, 550004, People's Republic of China

*These authors contributed equally to this work

Correspondence: Bailong Hu; Xiaohua Zou, Department of Anesthesiology, The Affiliated Hospital of Guizhou Medical University, No. 28 Guiyi Street, Yunyan District, Guiyang, Guizhou, 550004, People's Republic of China, Tel +86-13809416036, Fax +86-851-86771013, Email 375896605@qq.com; zouxiaohuazxh@163.com

Purpose: Sepsis can induce sepsis-associated encephalopathy (SAE), with Ulinastatin (UTI) serving a critical anti-inflammatory role. This study aimed to identify the hub genes in an SAE mouse model following UTI intervention and investigate the underlying molecular mechanisms.

Materials and Methods: Through differential expression analysis to obtain differentially expressed genes (DEGs), ie, UTI vs CLP (DEGs1) and Con vs CLP (DEGs2). After taking the intersection of the genes with opposite differential trends in these two parts and immune-related genes (IRGs), DE-IRGs were obtained. Hub genes in the protein-protein interaction (PPI) network were then determined using six algorithms from the Cytohubba plugin in Cytoscape. Gene set enrichment analysis (GSEA) was employed to explore the functional relevance of these hub genes. Additionally, the immune microenvironment across the three groups was compared, and hub gene-related drugs were predicted using an online database. Finally, qRT-PCR was used to validate the expression of the hub genes in hippocampal tissue from CLP mice.

Results: RNA sequencing obtained 864 differentially expressed genes (DEGs) (CLP vs Con) and 279 DEGs (UTI vs CLP). Taking the intersection of DEGs with opposite expression trends yielded 165 DEGs. Six key genes (ICAM - 1, IRF7, IL - 1β, CCL2, IL - 6 and SOCS3) were screened by six algorithms. Immune infiltration analysis found that Treg cells were reversed after treatment with UTI in the diseased state. A total of 106 hub - gene - related drugs were predicted, among which BINDARIT - CCL2 and LIFITEGRAST - ICAM1 showed particularly high affinities. The qRT - PCR verification results were consistent with the sequencing results.

Conclusion: In conclusion, *ICAM-1, IRF7, IL-1β, CCL2, IL-6*, and *SOCS3* were identified as potential therapeutic targets in SAE mice treated with UTI. This study offers theoretical support for UTI as a treatment option for SAE.

Keywords: sepsis-associated encephalopathy, ulinastatin, immune, Treg cells, RNA sequencing

Introduction

Sepsis is life-threatening organ dysfunction caused by a dysregulated host response to infection.[1–3] Between 30% and 70% of individuals diagnosed with sepsis are likely to develop sepsis-associated encephalopathy (SAE), a condition marked by widespread cerebral dysfunction.[4] SAE typically occurs in critically ill patients within intensive care units, where it often results in rapid mental decline, manifesting as cognitive impairment, confusion, disorientation, stupor, or coma.[5] Clinically, SAE has been linked to significantly worse prognoses, including an elevated risk of permanent neurocognitive deficits.[6,7] SAE further exacerbates mortality rates, increases in-hospital costs, and prolongs

hospitalization, often accompanied by persistent cognitive and physical limitations.[8] The pathogenesis of SAE is multifactorial, involving inflammatory cytokines, blood-brain barrier disruption, ischemic events, neurotransmitter imbalances, and mitochondrial dysfunction, though its precise mechanisms remain unclear.[9] Given this incomplete understanding, identifying reliable biomarkers is essential for early diagnosis, prevention, and further investigation into the disease's underlying mechanisms.

SAE perpetuates a vicious cycle of sepsis-induced immunosuppression.[10] Studies indicate that brain dysfunction in SAE is closely associated with immune dysregulation and impaired neuroendocrine-immune interactions, particularly those involving the cholinergic anti-inflammatory pathway, the hypothalamic-pituitary-adrenal axis, and the sympathetic nervous system.[10] This dysfunction in neural regulation compromises immune function, affecting critical immune cells such as neutrophils, macrophages/monocytes, dendritic cells, and T lymphocytes, thereby sustaining a destructive loop of brain damage and abnormal immune responses.[11] Investigating the immune-related mechanisms involved in SAE offers a promising pathway for the development of novel therapeutic strategies.

Ulinastatin (UTI), a broad-spectrum serine protease inhibitor, exhibits strong immunomodulatory properties, making it an effective agent for modulating inflammation and protecting vascular endothelial cells. This renders UTI a promising therapeutic option for conditions like sepsis and postoperative cognitive dysfunction.[12–14] Research has shown that UTI positively affects sepsis progression in mice by modulating both the quantity and function of regulatory T cells (Tregs) via the TLR4/NF-κB signaling pathway.[14] Furthermore, UTI may be employed alongside thymosin α1 (Tα1) in immunotherapeutic strategies to markedly enhance the modulation of inflammatory mediators in sepsis patients.[15] Additionally, UTI can be administered in conjunction with TIENAM to mitigate inflammation and modulate the immune response, thereby improving outcomes in murine models of sepsis induced by cecal ligation and puncture.[16] However, no current evidence supports UTI as a therapeutic drug for SAE, emphasizing the need to identify specific therapeutic targets to advance precision medicine, particularly for the Southeast Asian population.

Currently, no bioinformatics studies have explored UTI's impact on immune-related genes in SAE therapy. Therefore, this study aimed to identify candidate genes for UTI therapy in SAE mice using animal models and transcriptome sequencing. Hub genes were identified through the application of six algorithms within the context of protein-protein interaction (PPI) analysis. Following this, gene function analysis, immune infiltration analysis, and drug prediction were conducted, focusing on these hub genes. Finally, the diagnostic potential of these hub genes was validated using animal samples, confirming that UTI enhances the immune-inflammatory microenvironment in sepsis. This study offers critical insights into the diagnosis and treatment of SAE, serving as a significant reference for research and therapeutic interventions related to SAE diseases.

Materials and Methods
Grouping and Animal Model
Fifteen male C57 mice (6–8 weeks old, 20–22 g) were obtained from XX and housed in a sterile environment with adequate food and water. The mice were randomly assigned to three groups: Sepsis (CLP, n = 5), ulinastatin treatment (UTI, n = 5), and normal control (Con, n = 5). The mouse sepsis model was established using cecal ligation and puncture (CLP), as described in a previous study.[17] Within 12 hours post-surgery, the experimental group showed a marked decrease in activity, food, and water intake, with a mortality rate of approximately 40% at 24 hours. Under anesthesia, mice were placed on an operating table, and the mid-to-lower abdominal hair was shaved. After sterilization, a 1 cm incision was made along the ventral midline, and the cecum was gently manipulated with forceps. Three-quarters of the cecum was ligated at the base using sterile 3–0 silk. The intestinal contents were evacuated twice using an 18-G needle before the cecum was repositioned in the abdominal cavity. The incision was then sutured with four layers of mycelium thread and sterilized again. Mice in the control group underwent the same procedure without cecal ligation or puncture. Ulinastatin was dissolved in 0.9% saline and administered intravenously at 100,000 U/kg via the caudal vein, 1 hour before and 6 hours after the CLP procedure.[14] After 24 hours, hippocampal tissues were harvested and either stored at −80°C or fixed in 4% paraformaldehyde for subsequent analysis.

Neurobehavioral assessments were conducted on mice to evaluate their neural reflexes, thereby confirming the onset of SAE. As outlined in a prior study,[18] a score of "0" denoted an absence of reflexes, "1" indicated diminished reflexes, and "2" represented normal reflexes. A neurobehavioral score of < 6 is considered one of the diagnostic criteria for SAE.[19] The evaluated reflexes included the pinna reflex, corneal reflex, righting reflex, tail flexion, and escape response reflex.

Observation of Hippocampus Tissues Assessment Using Hematoxylin-Eosin Staining (HE) Staining

Pathological alterations in the hippocampal tissues were evaluated using HE staining. The entire brain specimen was fixed in paraformaldehyde, dehydrated through an alcohol gradient using an automated dehydration system, and embedded in paraffin for sectioning. The sections were then dewaxed, stained with hematoxylin and eosin, re-dehydrated, and mounted with neutral resin. Pathological alterations in the hippocampal tissues were observed using the BA210 Digital Trinocular Camera Microscopy System from Motic Industrial Group Co., Ltd., which was employed for image acquisition.

Morris Water Maze Test

As previously described, the Morris water maze test was utilized to assess spatial learning and memory across the three groups of mice.[20] This experiment was conducted 72 hours after CLP. The maze consists of a circular pool, 100 cm in diameter and 40 cm in height, filled with opaque water to a depth of 28 cm. The experiment spans five days: the first four days serve as the training phase. During this phase, each mouse is introduced into the water from one of the four quadrants at 20-minute intervals. Mice are given 60 seconds per trial to locate a hidden platform submerged 0.5 cm below the surface in the target quadrant. If a mouse fails to reach the platform within the time limit, it is guided manually to the platform, where it remains for 20 seconds before removal. On the fifth day, the platform is removed, and each mouse is tested in a 60-second trial. The number of entries into the target quadrant (where the platform was located) and the total time spent in that quadrant were recorded.

Y-Maze Test

The Y-maze test was conducted to evaluate spontaneous alternation behavior one day postoperatively. The Y-maze apparatus, made from grey plastic, consists of three identical arms positioned at 120° angles, with each arm measuring 50×10 × 40 cm. Mice were placed in the center of the maze and allowed to explore all three arms for 8 minutes. After each test, the maze was thoroughly cleaned with 75% ethanol. An arm entry was recorded when the mice placed all four paws inside an arm, and the sequence and total number of arm entries were documented via a digital camera.

$$Spontaneous\ alteration\ percentage\ =\ ((number\ of\ spontaneous\ alterations)/(total\ arm\ entries\ -\ 2))\ \times\ 100\%$$

Transcriptome Sequencing

Total RNA extraction was performed using the Trizol reagent (Thermo Fisher, 15596018) according to the manufacturer's instructions. Only high-quality RNA samples with a RIN above 7.0 were selected for sequencing library construction, following quantitative and qualitative assessment via the Bioanalyzer 2100 and RNA 6000 Nano LabChip Kit (Agilent, CA, USA, 5067–1511). After extraction, mRNA was isolated from 5 μg of total RNA using Dynabeads Oligo (dT) (Thermo Fisher, CA, USA) in a two-step purification process. The purified mRNA was fragmented into smaller pieces by exposure to divalent cations at elevated temperatures (Magnesium RNA Fragmentation Module, NEB, cat.e6150, USA) at 94°C for 5–7 minutes. Next, the fragmented RNA was reverse transcribed to generate cDNA using SuperScript™ II Reverse Transcriptase (Invitrogen, cat. no. 1896649, USA). The U-labeled second-strand DNA was synthesized from the cDNA libraries using E. coli DNA polymerase I (NEB, cat. no. M0209, USA), RNase H (NEB, cat. no. M0297, USA), and dUTP solution (Thermo Fisher, cat. no. R0133, USA). Subsequently, an adenine base was added to the blunt ends of each strand to prepare them for ligation with indexed adapters. Each adapter featured a T-base overhang to facilitate attachment to the A-tailed DNA fragments. The

fragments were then ligated with dual-index adapters, followed by size selection using AMPure XP beads. Following treatment with the heat-sensitive UDG enzyme (NEB, cat.m0280, USA), the U-labeled second-strand cDNA underwent PCR amplification, starting with initial denaturation at 95°C for 3 minutes, followed by 8 cycles of 98°C for 15 seconds, annealing at 60°C for 15 seconds, and extension at 72°C for 30 seconds, with a final extension at 72°C for 5 minutes. The final cDNA fragment insert size averaged 300±50 base pairs. Paired-end sequencing (2×150 bp) was conducted on an Illumina Novaseq™ 6000 (LC-Bio Technology Co., Ltd., Hangzhou, China) according to the manufacturer's protocol.

Data Quality Control and Preprocessing

Quality control of sequencing data was performed using FastQC (version 0.11.9), filtering out reads with adaptor contamination, low-quality bases, or undetermined nucleotides. Clean reads were generated using Trimmomatic (version 0.39). Alignment to the GRCm39 reference genome was executed with HISAT2, and transcript assembly and quantification of mRNA expression levels were achieved using StringTie (https://ccb.jhu.edu/software/stringtie) based on FPKM calculations.

$$FPKM = \frac{total\ exon\ fragments}{mapped\ reads\ (millions) \times exon\ length\ (kB)}.$$

The hierarchical clustering analysis was carried out using the R package stats (v. 4.2.2),[21] and principal component analysis (PCA) was performed using uwot package (v. 0.2.2)[22] to assess sample reproducibility.

Differential Expression Analyses

DEGs between the CLP and Con groups (CLP vs Con), referred to as C-DEGs, were identified using the DESeq2 package (v. 1.38.0).[23] Similarly, DEGs between the UTI and CLP groups (UTI vs CLP), labeled as U-DEGs, were screened. The selection criteria for both C-DEGs and U-DEGs were set as |$\log_2$fold change (FC)| > 0.8 and p-adj. < 0.05. The results were subsequently visualized with volcano plots using ggplot2 (v. 3.4.4)[24] and heatmaps created with the ComplexHeatmap (v. 2.16.0).[25] Genes showing opposite expression trends in both C-DEGs and U-DEGs were considered key DEGs post-UTI treatment, identified through intersection analysis via ggvenn (v. 0.1.10, https://github.com/yanlinlin82/ggvenn).

Identification of Differentially Expressed Immune-Related Genes (DE-IRGs)

A total of 1,793 immune-related genes (IRGs) were sourced from the ImmPort database (https://www.immport.org/shared/genelists)[26] and converted to 1,646 murine IRGs using the biomaRt (v. 2.58.0) package (https://grch37.ensembl.org/info/data/biomart/index.html). The intersection of key DEGs and these murine IRGs yielded DE-IRGs, identified with ggvenn (v. 0.1.10).

Function Enrichment Analyses

Functional enrichment analysis of DE-IRGs, including Gene Ontology (GO) and Kyoto Encyclopedia of Genes and Genomes (KEGG) pathway analyses, was performed using the clusterProfiler (v. 4.8.3) package (p-adj. < 0.05).[27] GO enrichment analysis encompassed biological processes (BP), molecular functions (MF), and cellular components (CC).

Protein-Protein Interaction (PPI) Network

A PPI network of DE-IRGs was constructed using the STRING database (https://string-db.org) (Interaction score = 0.4), and protein interactions were visualized. The CytoHubba plugin in Cytoscape (v. 3.9.1)[28] was employed to identify hub genes, applying six algorithms: maximal clique centrality (MCC), maximum neighborhood component (MNC), edge percolated component (EPC), degree, closeness, and betweenness. The top 10 DE-IRGs from each algorithm were overlapped to determine the final hub genes.

Gene Set Enrichment Analysis (GSEA) and Gene-Gene Interaction (GGI) Network

GSEA of the hub genes was conducted using the clusterProfiler (v. 4.8.3) package[27] to explore their potential functions. A total of 186 background gene sets were obtained from the MSigDB (v. 7.5.1) package (C2_CP:KEGG; Species: Mus musculus).[29] Spearman correlation analysis was then performed between the hub genes and all other genes using the corrplot (v. 0.92) package (https://github.com/taiyun/corrplot), ranking the correlation coefficients. GSEA was applied with thresholds of |normalized enrichment scores (NES)| > 1 and p-adj. < 0.05. Additionally, the top 20 genes related to the hub genes were predicted through the GeneMANIA database (http://genemania.org). A GGI network was constructed for the hub genes and their top 20 related genes, revealing their co-enriched potential pathways.

Evaluation of Infiltrating Immune Cells

To assess whether UTI treatment in sepsis mice induced alterations in the immune microenvironment of hippocampal tissues, immune cell infiltration analysis was conducted using the ImmuCellAI package (v. 0.1.0).[30] The infiltration levels of 36 immune cell types were visualized with ggplot2 (v. 3.4.4).[24] Differences in immune cell infiltration among groups were compared using the Wilcoxon test ($p < 0.05$). Additionally, Spearman correlation between hub genes and immune cells was examined (|cor| > 0.3, $p < 0.05$).

Molecular Regulatory Network

miRNAs associated with hub genes were retrieved from the miRDB database (https://mirdb.org/) based on a target score ≥ 80, while miRNAs were also predicted from the miRWalk database (http://129.206.7.150/) (binding point = 1). Hub miRNA-mRNA pairs were determined by intersecting the miRNAs identified by both databases. Transcription factors (TFs) related to hub genes were predicted using the iRegulon plugin in Cytoscape (v. 3.9.1)[28] with NES > 5. Based on the hub miRNA-mRNA and TF-mRNA pairs, a TF-mRNA-miRNA regulatory network was constructed.

Potential Drugs Prediction and Molecular Docking

To identify potential therapeutic drugs for sepsis, drug-gene interactions were retrieved from the DGIdb database (http://www.dgidb.org/) (FDA-approved and immunotherapies), using hub genes as keywords. A drug-gene network was established based on these interactions, and key drugs were identified with an interaction score > 2. Spearman correlation analysis was then conducted between hub genes and key drugs (|cor| > 0.3, $p < 0.05$). For drugs with an interaction score > 5, their 3D structures were obtained from the PubChem database (https://pubchem.ncbi.nlm.nih.gov/). The 3D protein structures of hub genes were acquired from the RCSB Protein Data Bank (RCSB PDB, http://www.pdb.org/). Docking simulations with core targets were performed using Autodock-vina (v. 1.5.7),[31] and the results were visualized using PyMol (v. 2.5.5) (https://pymol.org/) and proteins.plus (https://proteins.plus/).

Validation of Quantitative Real-Time Polymerase Chain Reaction (qRT-PCR)

To verify the reliability of hub gene expression results, qRT-PCR was carried out on 15 frozen hippocampal tissue samples (5 sham, 5 control, and 5 UTI samples).

Total RNA was extracted from mouse hippocampal tissue using the TriQuick Reagent kit (Beijing Solaibao Technology Co., LTD, China). Reverse transcription was performed with the PrimeScript™ RT reagent kit (Takara, Bao Bioengineering (Dalian) Co., Ltd., Dalian, China), and quantitative PCR was conducted using TB Green Premix Ex Taq II on a real-time fluorescence quantitative PCR system. The thermal cycling protocol included an initial denaturation step at 95°C for 30 seconds, followed by 40 cycles of 95°C for 5 seconds and 60°C for 30 seconds. The expression levels of Icam1, Irf7, Il1b, Ccl2, Il6, and Socs3 in the hippocampal samples were quantified. GraphPad Prism 5 was used for plotting and statistical analysis to assess significant differences. GAPDH served as the internal reference gene. The primers used for each key gene are listed in Table 1.

Enzyme-Linked Immunosorbent Assay (Elisa)

Serum medium concentrations of cytokines, including IL-6, IL-1β, were measured using the quantitative ELISA kits according to the manufacturer's instructions. The optical density was measured at 450 nm. The standard curve of each cytokine determined the cytokine concentrations.

Table 1 Primers for qRT-PCR Used in the Current Study

Primer		Sequence
ICAM-1	Forward (5′-3′)	TGGAGACGCAGAGGACCTTAAC
	Reverse (5′-3′)	CGACGCCGCTCAGAAGAAC
IRF7	Forward (5′-3′)	TGAGCGAAGAGAGCGAAGAGG
	Reverse (5′-3′)	CGTACACCTTATGCGGATCAACTG
IL-6	Forward (5′-3′)	GAGAGGAGACTTCACAGAGGATACC
	Reverse (5′-3′)	TCATTTCCACGATTTCCCAGAGAAC
IL-1β	Forward (5′-3′)	AATCTCGCAGCAGCACATCAAC
	Reverse (5′-3′)	AGGTCCACGGGAAAGACACAG
CCL2	Forward (5′-3′)	ACTGCATCTGCCCTAAGGTCTTC
	Reverse (5′-3′)	TCACTGTCACACTGGTCACTCC
SOCS3	Forward (5′-3′)	TCTTTGCCACCCACGGAACC
	Reverse (5′-3′)	TCAGTACCAGCGGAATCTTCTCG
β-actin	Forward (5′-3′)	TATGCTCTCCCTCACGCCATCC
	Reverse (5′-3′)	GTCACGCACGATTTCCCTCTCAG

Abbreviations: SAE, sepsis-associated encephalopathy (SAE); UTI, Ulinastatin; GEO, gene expression omnibus; DEGs, differentially expressed genes; IRGs, immune-related genes; DE-IRGs, differential expressed immune-related genes; GSEA, Gene set enrichment analysis; PPI, protein-protein interaction; Tregs, regulatory T cells; CLP, Cecal ligation and puncture; HE, hematoxylin eosin; MWM, Morris Water Maze; PCA, principal component analysis; GO, Gene Ontology; KEGG, Kyoto Encyclopedia of Genes and Genomes; BP, biological process; CC, cellular components; MF, molecular functions; MCC, maximal clique centrality; MNC, maximum neighborhood component; EPC, edge percolated component; GGI, gene-gene interaction; TFs, transcription factors; Dgidb, Drug–Gene Interaction Database (DGIdb); qRT-PCR, quantitative real-time polymerase chain reaction; DG, dentate gyrus; TNF, tumor necrosis factor; BBB, Blood-brain barrier; TLR4, Toll-like receptor 4.

Statistical Analysis

All statistical analyses were performed using R software (v. 4.3.1), with $p < 0.05$ considered statistically significant (two-tailed).

Results

Ulinastatin Can Alleviate Hippocampal Neuron Damage, Improve Neurobehavioral Manifestations and Peripheral Inflammation in Mice with Sepsis

Hippocampal tissue HE staining and light microscopy were performed 24 hours after CLP to evaluate postoperative morphological changes in neurons within the dentate gyrus (DG) of the mouse hippocampus (Figure 1). In the Con group, neurons appeared with normal morphology, including abundant cell numbers, well-defined boundaries, regular arrangement, large, round nuclei, and distinct nucleoli (Figure 1A). Conversely, the DG region in the CLP group showed significant neuronal damage, characterized by shrunken and hyperchromatic neurons, poorly defined nuclear boundaries, disorganized arrangement, and evident neuronal shrinkage and necrosis (Figure 1B, black arrows). Following UTI treatment, the number of shrunken and necrotic neurons in the DG was markedly reduced compared to the CLP group (Figure 1C, black arrows), suggesting that UTI mitigates hippocampal neuronal injury in septic mice.

Furthermore, we conducted an assessment of the neurobehavioral performance across three distinct groups of mice (Figure 1D). The findings indicated a progressive decline in neurobehavioral scores within the CLP group following awakening, with the lowest scores observed at 24 hours post-surgery. In contrast, the Con group consistently maintained a stable score of 10. Additionally, the UTI group exhibited significantly higher scores compared to the CLP group. Based on established SAE evaluation criteria, no instances of SAE were identified in either the Con or UTI groups, the CLP group demonstrated a 70% incidence of SAE, and only those mice diagnosed with SAE were included in subsequent experimental analyses.
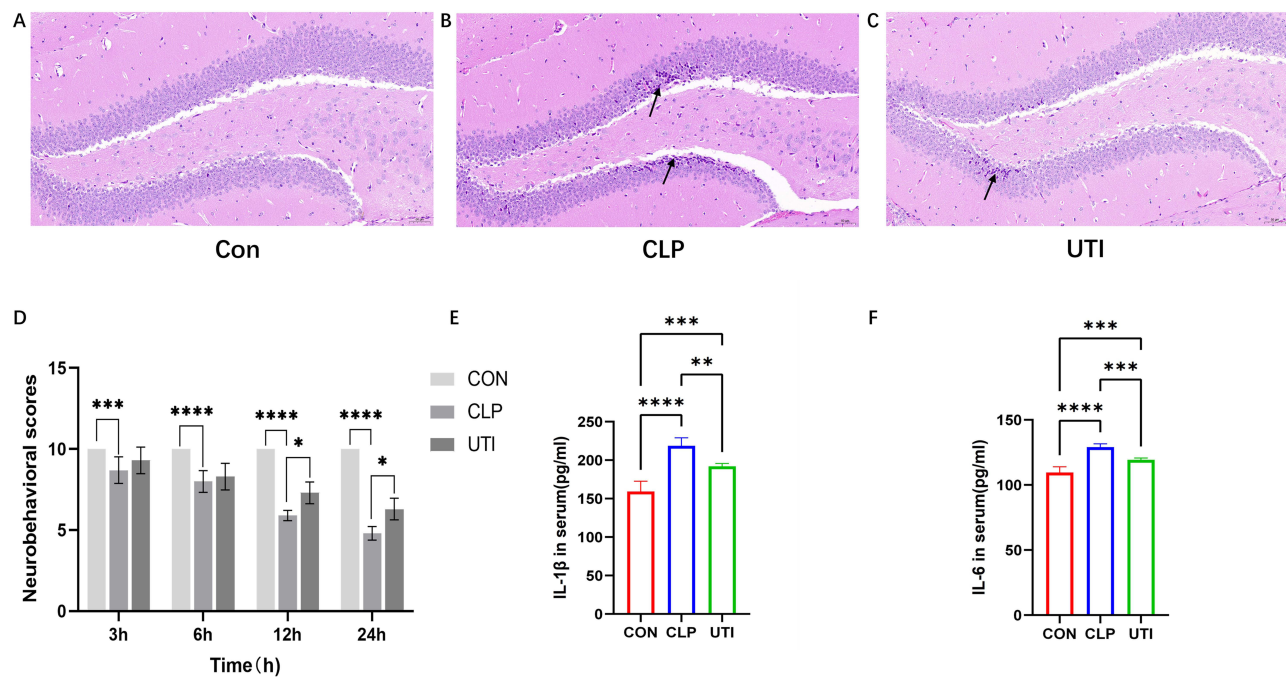
Figure I Effects of UTI on Hippocampal Neurons, Neurobehavioral Performance and Inflammatory Cytokines in Septic Mice. (**A–C**) Representative images of HE-stained hippocampal sections from each group. Black arrows indicate nuclear disorder, neuronal shrinkage, and necrosis. Magnification:×20. (**D**) Neurobehavioral score. Data is represented by histograms. Values are expressed as mean ± SEM (n = 10 in each group). (**E** and **F**) The comparisons of IL-1β, IL-6 in serum in different groups. * $p<0.05$, ** $p<0.01$, *** $p<0.001$, **** $p<0.0001$, n=6.

To evaluate the therapeutic efficacy of UTI on inflammation, serum levels of the proinflammatory cytokines IL-6 and IL-1β were quantified using ELISA. The results demonstrated that the serum concentrations of IL-6 and IL-1β were elevated in the CLP group; however, these levels were significantly reduced following UTI treatment. These findings suggest that UTI treatment has the potential to attenuate inflammation in murine models of sepsis. (Figure 1E and F).

Ulinastatin Can Improve Learning and Cognitive Functions in Mice with SAE

The experimental schedule is outlined in Figure 2A. Hippocampus-dependent spatial learning and memory were evaluated in each group using the Morris Water Maze (MWM) test. Figure 2B shows representative swimming paths on the final day of training. Throughout the 4-day training period, mice in the CLP group exhibited a significantly longer escape latency on day 4 compared to the Con group. However, UTI treatment substantially reduced escape latency in the CLP group (Figure 2C). Additionally, the CLP group demonstrated less time spent in the target quadrant and fewer platform crossings, both of which were restored by UTI treatment (Figure 2D and E). The Y-maze test was also employed to evaluate hippocampal spatial working memory, showing that the CLP group had a lower percentage of spontaneous alternation compared to the Con group, while UTI treatment improved this percentage (Figure 2F). These results suggest that UTI ameliorates cognitive deficits in SAE mice.

A Total of 51 DE-IRGs Were Identified

In the transcriptomic analysis, PCA of samples from the CLP (n = 5), UTI (n = 5), and Con (n = 5) groups confirmed no outliers (Figures 3A and S1). Differential expression analysis revealed 864 C-DEGs (CLP vs Con; 637 up-regulated and 227 down-regulated) and 279 U-DEGs (UTI vs CLP; 114 up-regulated and 165 down-regulated) (Figure 3B–E). An overlap analysis identified 165 key DEGs attributed to UTI treatment (Figure 3F). Additionally, 51 DE-IRGs were identified by intersecting these 165 key DEGs with 1,646 murine IRGs (Figure 3G).

The DE-IRGs Were Co-Enriched in the Immunoinflammatory Process

Functional enrichment of DE-IRGs was examined through GO and KEGG analyses. In GO analysis, 1,342 GO terms were significantly enriched (*p*-adj. < 0.05), including 1,221 BP terms, 38 CC terms, and 83 MF terms, with 19 DE-IRGs
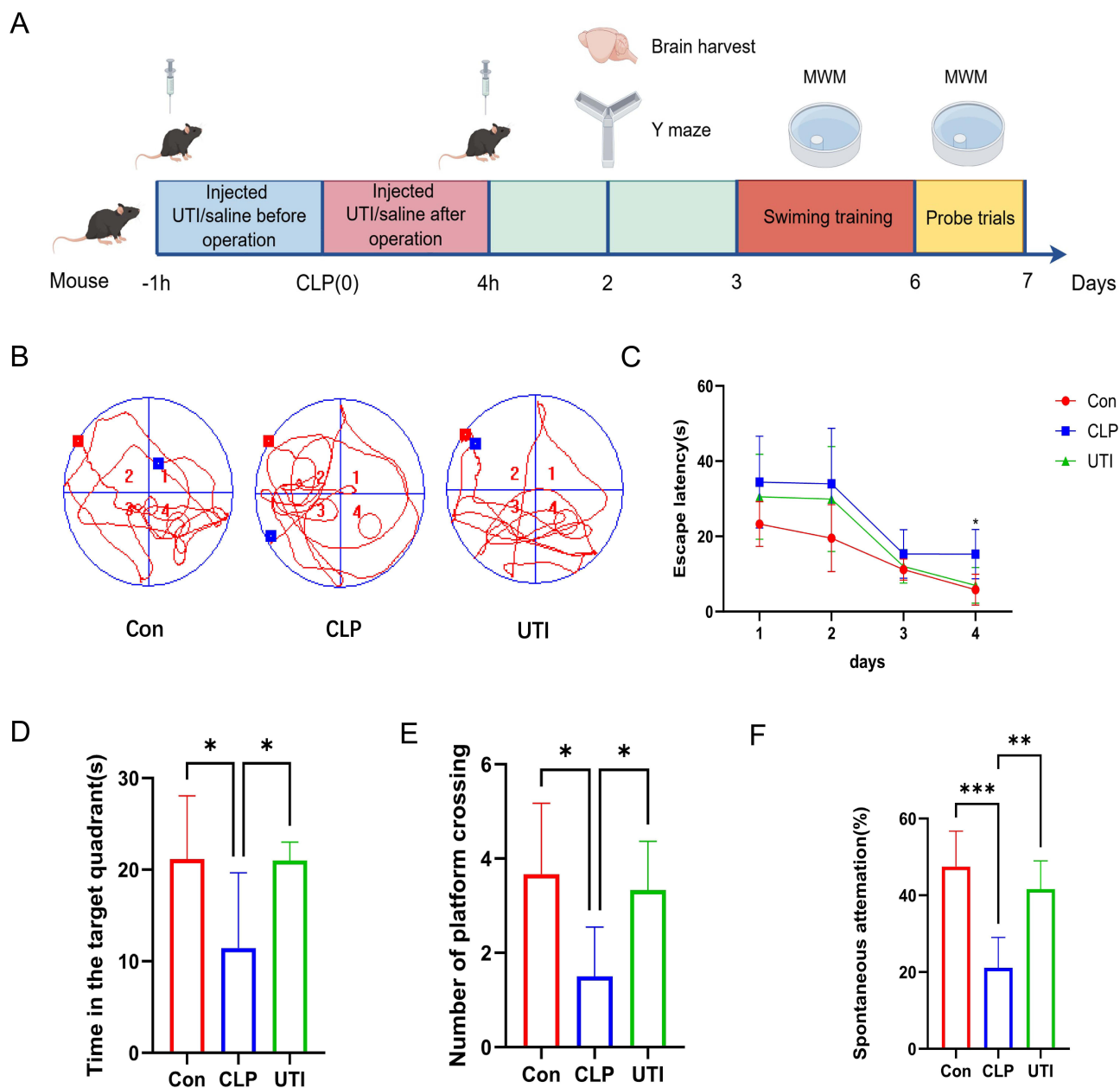
Figure 2 UTI ameliorates cognitive impairment in SAE mice. (**A**) The experimental flow of animal model construction. (**B**) Representative movement trajectories of each group on the final day of the MWM test. (**C**) Escape latency times in the MWM test across all groups. (**D**) Time spent in the target quadrant during the testing phase for each group. * $p < 0.05$, n = 6. (**E**) Number of platform crossings in the testing phase for each group. * $p < 0.05$, n = 6. (**F**) Spontaneous alternation in the testing phase for each group. ** $p < 0.01$, *** $p < 0.001$, n = 6.

involved in cytokine-mediated signaling pathways (Figure 4A and Table S1). In KEGG analysis, 50 pathways were significantly enriched (*p*-adj. < 0.05), including the TNF signaling pathway, Influenza A, and Epstein-Barr virus infection, among others (Figure 4B and Table S2).

A Total of Six Hub Genes Were Identified by the Cytohubba Plugin

Initially, a PPI network consisting of 49 nodes and 401 edges was constructed (Figure 5A). Among the interactions, the pairs Fcer1g-Syk, Il13ra1-Il4ra, Il1a-Il1b, Il2rg-Il4ra, and Lcp2-Syk exhibited the highest combined scores (combined score = 0.999) (Table S3). Following this, the top 10 DE-IRGs identified by each algorithm were illustrated (Figure 5B–G). Through overlapping analysis, six hub genes were identified: *ICAM-1, IRF7, IL-1β, CCL2, IL-6,* and *SOCS3*
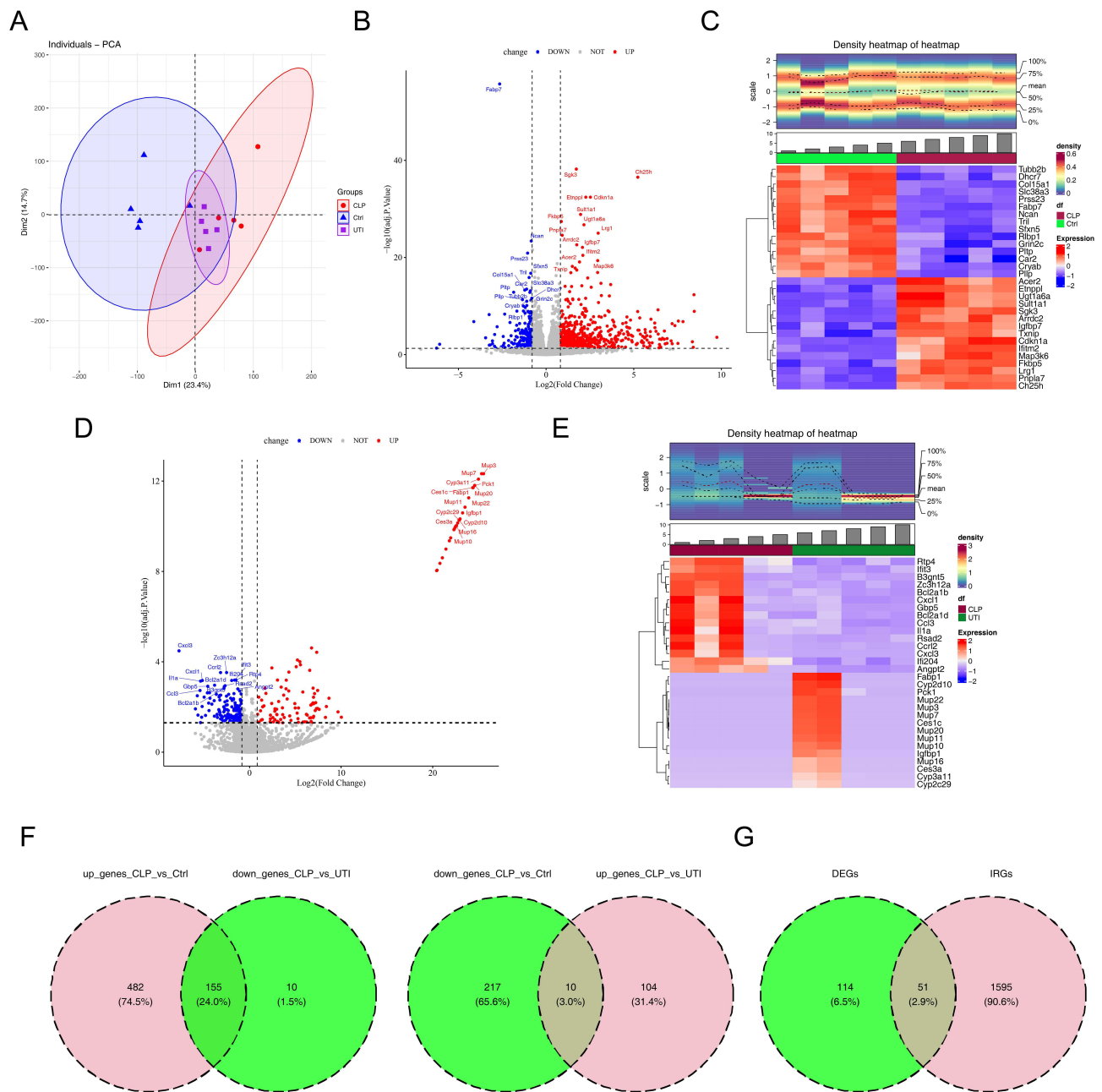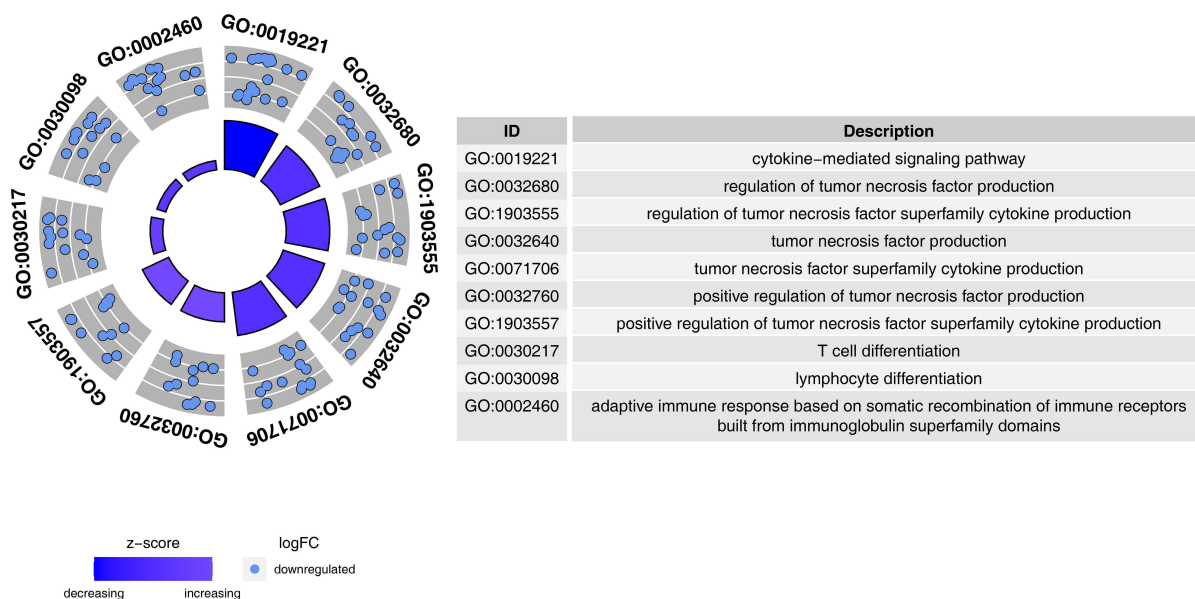
Figure 3 Identification of immune-related differentially expressed genes (DE-IRGs). (**A**) Principal Component Analysis. (**B**) Volcano plot depicting DEGs between CLP and control groups. (**C**) Heatmap illustrating DEGs between CLP and control groups. (**D**) Volcano plot of DEGs between CLP and UTI groups. (**E**) Heatmap of DEGs between CLP and UTI groups. (**F**) Venn diagram of differentially expressed genes (DEGs) among control, CLP, and UTI groups. (**G**) Venn diagram showing the overlap between IRGs and DEGs.

(Figure 5H). A GGI network was subsequently constructed based on these hub genes and the top 20 related genes, which are involved in processes such as cytokine receptor binding and leukocyte migration (Figure 5I). Notably, GSEA results revealed that the six hub genes were co-enriched in pathways related to NK cell-mediated cytotoxicity, leishmaniasis infection, and apoptosis (Figure 6).

The Infiltration of Treg Cells Was Increased After UTI Treatment

Immune cell infiltration was analyzed across three groups (Figure 7A), with granulocytes consistently scoring the highest in all groups. Between the CLP and Con groups, nine immune cell types showed significant differences in infiltration ($p <$
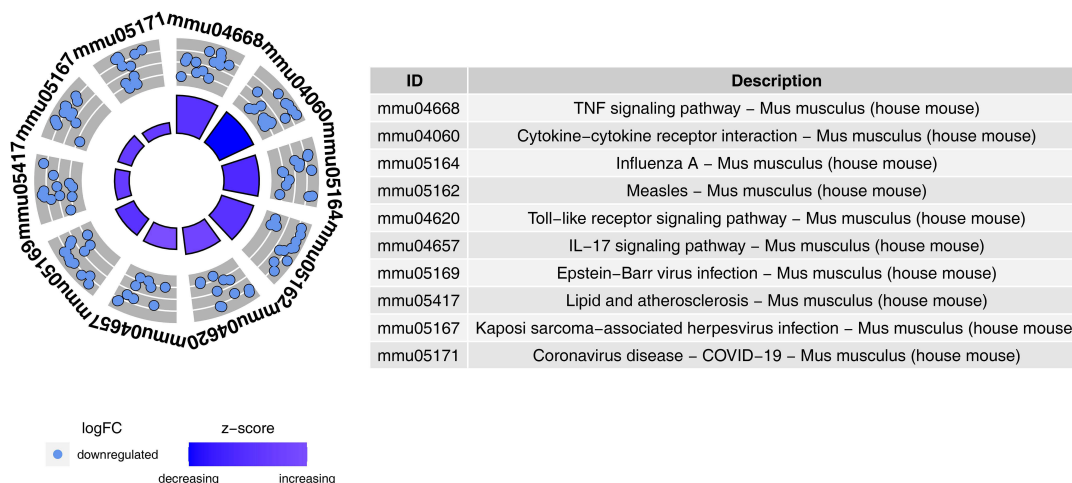
A

ID	Description
GO:0019221	cytokine–mediated signaling pathway
GO:0032680	regulation of tumor necrosis factor production
GO:1903555	regulation of tumor necrosis factor superfamily cytokine production
GO:0032640	tumor necrosis factor production
GO:0071706	tumor necrosis factor superfamily cytokine production
GO:0032760	positive regulation of tumor necrosis factor production
GO:1903557	positive regulation of tumor necrosis factor superfamily cytokine production
GO:0030217	T cell differentiation
GO:0030098	lymphocyte differentiation
GO:0002460	adaptive immune response based on somatic recombination of immune receptors built from immunoglobulin superfamily domains

B

ID	Description
mmu04668	TNF signaling pathway – Mus musculus (house mouse)
mmu04060	Cytokine–cytokine receptor interaction – Mus musculus (house mouse)
mmu05164	Influenza A – Mus musculus (house mouse)
mmu05162	Measles – Mus musculus (house mouse)
mmu04620	Toll–like receptor signaling pathway – Mus musculus (house mouse)
mmu04657	IL–17 signaling pathway – Mus musculus (house mouse)
mmu05169	Epstein–Barr virus infection – Mus musculus (house mouse)
mmu05417	Lipid and atherosclerosis – Mus musculus (house mouse)
mmu05167	Kaposi sarcoma–associated herpesvirus infection – Mus musculus (house mouse)
mmu05171	Coronavirus disease – COVID–19 – Mus musculus (house mouse)

Figure 4 Functional analysis of immune-related DE-IRGs. (**A**) GO term enrichment of DE-IRGs.(**B**) KEGG pathway enrichment of DE-IRGs.

0.05) (Figure 7B), while two immune cell types differed between the UTI and CLP groups ($p < 0.05$) (Figure 7C). Among these, only Treg cells were reduced in the CLP group compared to the Con group, but increased following UTI treatment (UTI vs CLP). Moreover, Treg cells displayed significant negative correlations with all hub genes except Irf7 (Figure 7D).

BINDARIT-Ccl2 and LIFITEGRAST-Icam1 had High Affinity

A total of 76 miRNA-mRNA pairs were identified from the miRDB database, while 1,960 pairs were retrieved from the miRWalk database. Fourteen hub miRNA-mRNA pairs were confirmed by intersecting the two datasets (Figure 8A). Additionally, 11 TFs related to the six hub genes were predicted, although no TFs were associated with Irf7. The resulting TF-mRNA-miRNA regulatory network included interactions such as Hcfc2-Socs3-mmu-miR-7002-3p, Stat4-Il1b-mmu-miR-7064-5p, and Foxp4-Icam-mmu-miR-12181-3p (Figure 8B). A total of 106 hub gene-related drugs were predicted, comprising 116 drug-gene interactions, though none were associated with Irf7 (Table S4). A drug-gene network was constructed for the remaining five hub genes (Figure 8C), with CARLUMAB-Ccl2, EMAPTICAP PEGOL-Ccl2, and ALICAFORSEN-Icam1 exhibiting the highest interaction scores (interaction score = 19.66). Among drugs
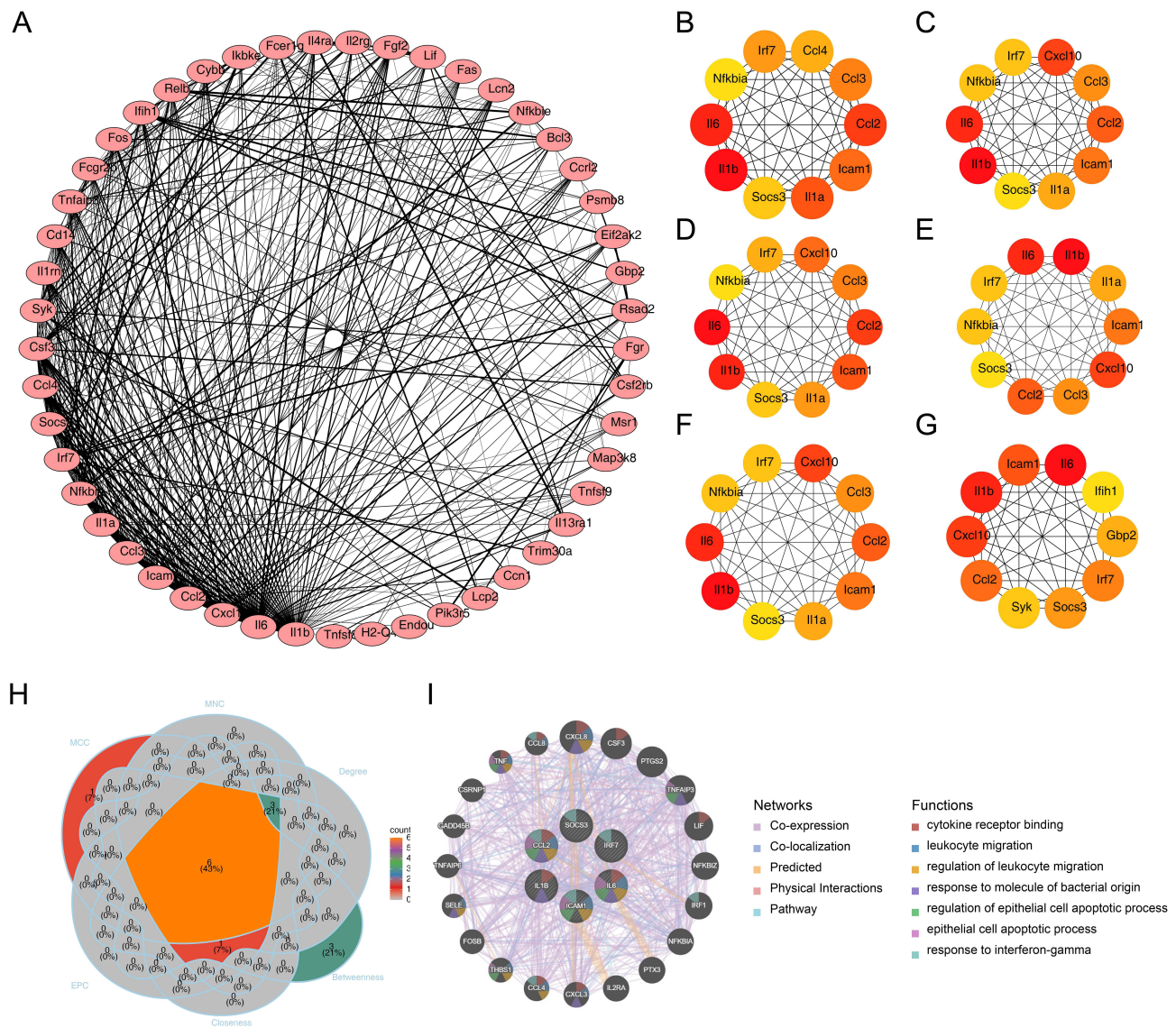
Figure 5 Hub gene screening using Cytohubba. (**A**) Protein-protein interaction network of DE-IRGs. (**B**) Top 10 DE-IRGs ranked by MCC. (**C**) Top 10 DE-IRGs ranked by MNC. (**D**) Top 10 DE-IRGs ranked by EPC. (**E**) Top 10 DE-IRGs ranked by Degree. (**F**) Top 10 DE-IRGs ranked by Closeness. (**G**) Top 10 DE-IRGs ranked by Closeness. (**H**) Intersection of top 10 hub genes across six algorithms. (**I**) Gene-gene interaction network of hub genes and top 20 related genes.

with interaction scores above 5, only BINDARIT and ENLIMOMAB PEGOL were retrieved. Molecular docking analysis revealed strong affinities for BINDARIT-Ccl2 (binding energy = −6.9 kcal/mol) and LIFITEGRAST-Icam1 (binding energy = −9.0 kcal/mol) (Figure 8D and E).

Expression Validation of the six Hub Genes

qRT-PCR validation confirmed that the expression levels of the six hub genes were consistent with the sequencing results. All six genes were significantly upregulated in the hippocampal tissue of the CLP group compared to the control group, while their expression was downregulated in the UTI group relative to the CLP group (Figure 9).

Discussion

SAE represents a significant complication of sepsis, affecting a large proportion of patients and contributing to higher mortality rates and poor outcomes. The lack of effective therapeutic options for SAE remains a critical challenge.[32] Studies have shown that immune response dysregulation plays a pivotal role in SAE development.[1] UTI functions as an

Figure 6 Gene set enrichment analysis (GSEA) of the six hub genes.
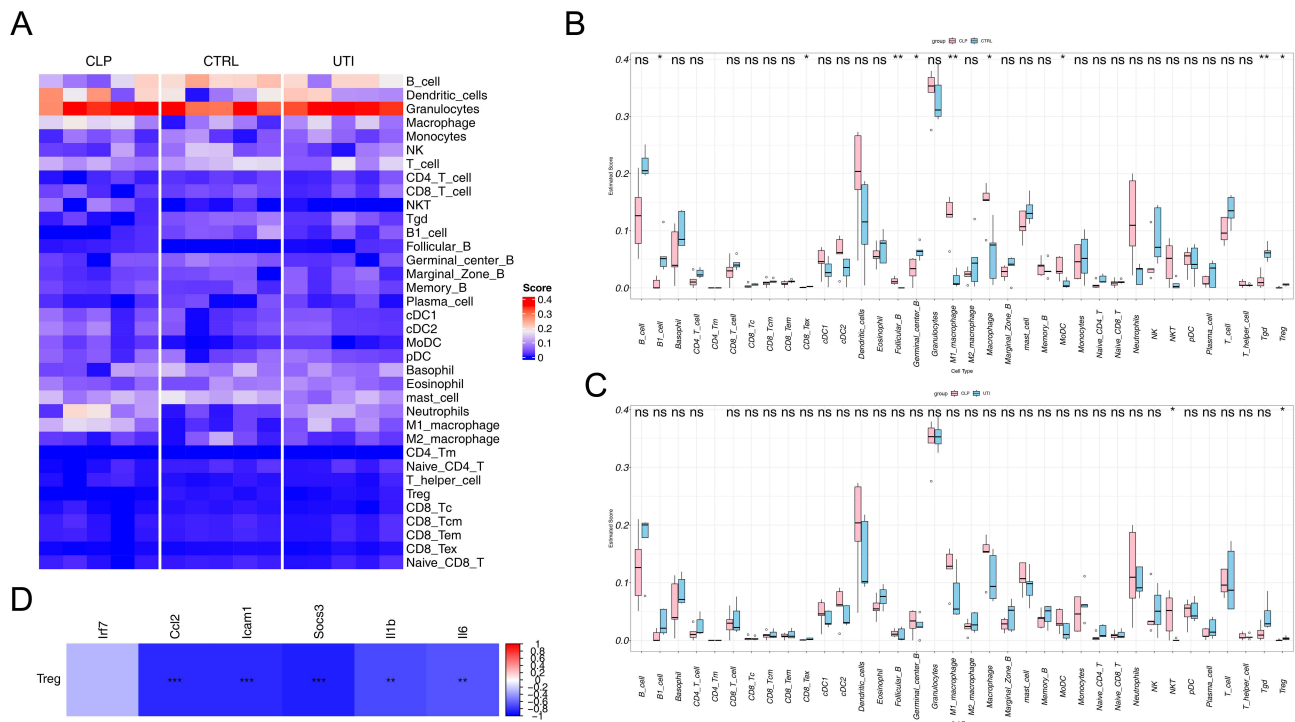

Figure 7 Immune cell infiltration analysis across the three groups. (**A**) Heatmap showing the distribution of 36 immune cell types in each sample. (**B**) Differential analysis of 36 immune cell types between the control and CLP groups. (**C**) Differential analysis of 36 immune cell types between the CLP and UTI groups. (**D**) Correlation analysis between the six hub genes and Treg cells. * *p*<0.05, ** *p*<0.01, *** *p*<0.001.
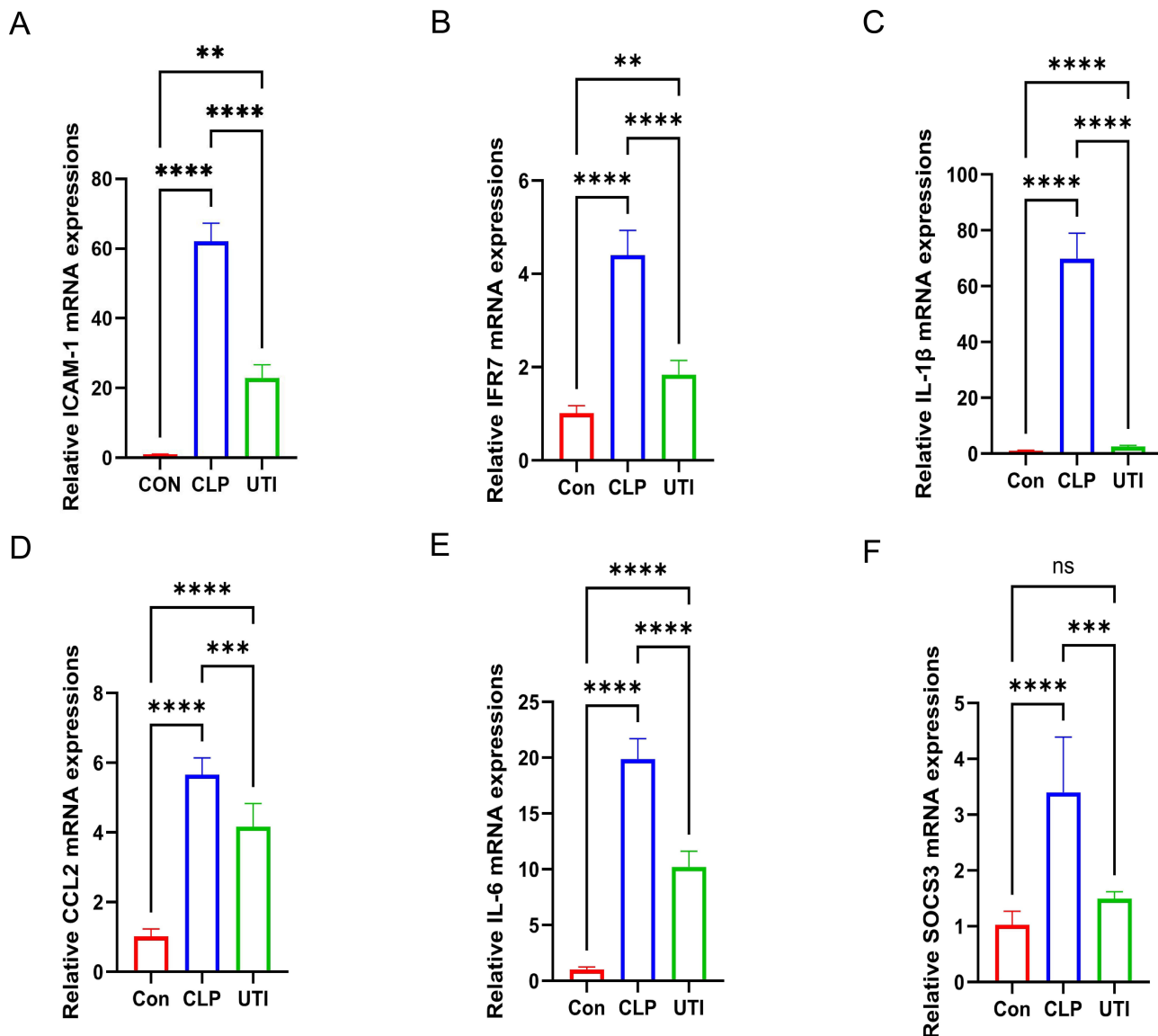
Figure 8 Prediction of potential therapeutic drugs targeting the six hub genes. (**A**) Venn diagram of common mRNA-miRNA interaction pairs predicted for the six hub genes. (**B**) TF-mRNA-miRNA regulatory network of the six hub genes. The green octagon represents a TF, the blue V represents a miRNA, and the purple oval represents a biomarker. (**C**) Drug-target network of the six hub genes. (**D**) Molecular docking results of BINDARIT with *CCL2*. (**E**) Molecular docking results of LIFITEGRAST with *ICAM1*..

Figure 9 Validation of mRNA expression levels for the six hub genes. (**A–F**) qRT-PCR validation of ICAM-1, IRF7, IL-1β, CCL2, IL-6, and SOCS3 expression. ** *p* < 0.01, *** *p* < 0.001, **** *p* < 0.0001, ns indicates not significant, n = 3–6.

immunomodulator that specifically targets the NLRP3 pathway in neurological disorders,[33] aiming to mitigate myocardial damage induced by sepsis through the inhibition of NLRP3 inflammasome activation.[34] While UTI has proven beneficial in treating sepsis by modulating immune function,[35] its potential application in SAE management has yet to be explored. This study employed UTI in a sepsis mouse model, performing an in-depth transcriptomic analysis of hippocampal tissue, which revealed six key immune-related genes associated with UTI treatment in SAE: *ICAM-1, IRF7, IL-1β, CCL2, IL-6*, and *SOCS3*. The expression levels of these genes were further validated through qRT-PCR. Moreover, Treg cells were identified as significant immune cells involved in UTI-mediated SAE treatment, offering a novel bioinformatics-based immune perspective on ulinastatin's therapeutic potential for SAE.

Six immune hub genes involved in UTI treatment of SAE were identified. *ICAM-1*, a glycoprotein and adhesion receptor found on endothelial and immune cells,[36] plays a critical role in mediating cell adhesion. Its main function is to facilitate the recruitment of leukocytes and immune cells to sites of inflammation, making it essential in inflammatory responses and the pathogenesis of immune-mediated diseases.[37] Studies show that plasma levels of *ICAM-1* are significantly elevated in patients with SAE compared to non-SAE individuals, suggesting it could serve as

a biomarker for predicting cognitive dysfunction in patients with sepsis.[38,39] Additionally, *ICAM-1* expression increases in endothelial and immune cells under inflammatory conditions,[40] which is consistent with our findings of elevated ICAM-1 levels in the hippocampal tissue of septic mice, implying a possible link between increased hippocampal *ICAM-1* expression and SAE. *IRF7*, a key transcription factor, regulates type I interferon production and innate immune responses. It is critical in modulating the IFN-I/III signaling pathway, contributing to host defense against viral infections and immunoregulation.[41] In sepsis, *IRF7* can upregulate Srg3 expression, leading to enhanced ferroptosis and M1 macrophage polarization, worsening septic lung injury.[42] Our study also observed upregulation of *IRF7* in the hippocampal tissue of SAE mice, indicating that *IRF7* transcriptional upregulation may be a contributing factor in SAE pathogenesis. *IL-1β*, a major pro-inflammatory cytokine involved in innate immune responses, plays a pivotal role in activating microglia and inducing neuroinflammation in SAE.[43] Our findings corroborate this, showing *IL-1β* upregulation in the hippocampal tissue of SAE mice. Likewise, *CCL2/MCP-1*, an early cytokine triggered by LPS-induced inflammation, is highly expressed in the brain during sepsis and contributes to SAE development.[44,45] Our study supports this observation, noting high *CCL2* expression in the hippocampal tissue of septic mice. *IL-6* is a key inflammatory mediator in sepsis and a useful biomarker for diagnosing the condition.[46,47] Research by Jiang et al demonstrated that inhibiting *IL-6* trans-signaling improves survival in septic mice and may offer a potential therapeutic approach for SAE.[20] UTI treatment was also shown to downregulate *IL-6* in the hippocampal tissue, reinforcing its potential role in SAE treatment. *SOCS3*, a member of the SOCS family, is inducible by inflammatory factors and plays a role in inhibiting immune response signaling.[48] Li et al suggested that *SOCS3* could serve as a diagnostic and therapeutic target for SAE and hepatic encephalopathy due to its association with immune cells, further supporting our research conclusions.[49] In summary, these six immune-related genes are upregulated and play critical roles in conditions such as sepsis and SAE, providing a solid theoretical foundation for our predictions. Prior research has demonstrated that individuals who survive sepsis frequently display anxiety-like behaviors, heightened activity of the hypothalamic-pituitary-adrenal (HPA) axis, and ongoing systemic and neuroinflammation. Despite the administration of corticosteroids, such as corticosterone, during the septic episode, these symptoms persist and may adversely impact object memory in female mice, while also enhancing their active coping behaviors. Furthermore, corticosterone treatment significantly modified the expression profiles of numerous genes within the hippocampus, notably resulting in the coordinated downregulation of activity-dependent genes.[50] A separate study demonstrated significant alterations in gene expression within the hippocampus of rats subjected to sepsis, observed 4.5 hours following LPS administration. Notably, there was an up-regulation of chemokines and endothelial cell-specific molecules. In contrast, norepinephrine treatment resulted in only a slight up-regulation of chemokine expression, while treatment with the inducible nitric oxide synthase inhibitor, 1,400 W, exhibited minimal impact on gene expression.[51] These studies offer significant insights into the alterations in hippocampal gene expression associated with SAE, thereby establishing a theoretical framework for investigating the precise molecular mechanisms by which UTIs regulate these genes in SAE.

Gene expression is closely linked to alterations in behavior. The research demonstrated that ICAM-1 conferred neuroprotection against amyloid beta-induced damage by inhibiting NF-κB, which subsequently led to enhanced cognitive performance in 5xFAD mice.[52] Furthermore, research has indicated that IL-6 plays a role in neural signaling associated with "sickness behavior", leading to behavioral alterations such as reduced appetite and diminished activity levels.[53] Currently, there are no documented studies examining the impact of IRF7, IL-1β, CCL2, and SOCS3 on behavior. In this investigation, mice with sepsis treated with UTI exhibited notable behavioral alterations. Concurrently, the expression profiles of these four biomarkers demonstrated significant modifications following UTI treatment. Consequently, it is hypothesized that these genes may play a crucial role in the behavioral changes associated with SAE. However, further research is required to elucidate the specific mechanisms involved.

GSEA and GeneMANIA analyses of six immune-related genes revealed their enrichment in NK cell-mediated cytotoxicity, JAK/STAT signaling, and Toll-like receptor (TLR) signaling pathways. The NK cell-mediated cytotoxicity pathway is implicated in sepsis pathogenesis by amplifying inflammation and contributing to organ damage.[54,55] This suggests that it may also play a role in SAE development by interacting with immune-related genes. The JAK-STAT pathway plays a critical role in modulating immune responses during sepsis.[56] Research indicates that *ICAM1* expression impacts blood-brain barrier (BBB) permeability,[57] with elevated levels during sepsis exacerbating its disruption.[58] The

JAK-STAT pathway may enhance endothelial cell function by downregulating *ICAM1* expression,[59,60] suggesting a potential role in modulating BBB permeability and SAE *via ICAM1* regulation. *SOCS3*, a well-established negative regulator of the JAK-STAT pathway,[61] has been identified as a therapeutic target for improving sepsis and SAE outcomes by inhibiting JAK-STAT signaling,[62] thereby mitigating sepsis-induced multiple organ failure and reducing inflammatory mediator release.[63] Toll-like receptors are key in pathogen recognition and immune activation.[64] In LPS-induced SAE mouse models, activation of the TLR4 signaling pathway in microglial cells exacerbates SAE,[65] while this activation is dependent on the transcriptional expression of *IRF7*.[66] The TLR signaling pathway has also been shown to stimulate *CCL2* activation in renal tubular epithelial cells, aggravating sepsis-induced renal injury.[67] Furthermore, TLR pathway activation increases the secretion of *IL-1β* and *IL-6*, intensifying inflammation and advancing sepsis progression.[68,69] Modulating the TLR pathway may offer a therapeutic avenue for addressing SAE by targeting *IRF7, CCL2, IL-1β*, and *IL-6*. SAE, characterized by inflammatory dysregulation, is also associated with GO terms such as cytokine receptor binding, leukocyte migration, and the regulation of leukocyte migration, all linked to the six key immune genes. Furthermore, the study identified that SAE mice exhibited not only pronounced behavioral abnormalities but also an up-regulation of inflammatory cytokines in the hippocampus, accompanied by morphological alterations. This finding further substantiates the strong correlation between SAE and the dysregulation of inflammatory processes. Concurrently, various metabolic pathways, including those involved in lipid metabolism, amino acid metabolism, glucose metabolism, and nucleotide metabolism, as well as inflammatory pathways and synaptic dysregulation, were intimately linked to hippocampal dysfunction in the early stages of SAE. The disruption of these metabolic pathways may exacerbate the progression of SAE by impairing the normal function of the hippocampus. Consequently, when investigating treatment strategies for SAE, it is imperative to consider the alterations in these metabolic pathways. This approach will enhance our understanding of the pathophysiological mechanisms underlying SAE and contribute to the development of more effective therapeutic interventions.[70] In conclusion, these immune genes play pivotal roles in pathways related to infection, immunity, and inflammation, significantly influencing the progression of SAE.

Previous studies have demonstrated that UTI can alleviate sepsis and related conditions by reducing inflammation, modulating immune cell activity, and protecting vascular endothelial cells through its effects on the JAK-STAT and TLR pathways.[71–74] UTI has also been shown to lower *ICAM-1* expression in endothelial cells,[75] and reducing *ICAM-1* levels in cerebral vessels and leukocytes has been associated with improved BBB integrity in septic mice and SAE.[76] Our findings suggest that UTI may decrease *ICAM-1* expression in the hippocampal tissue of septic mice, with *ICAM-1* being enriched in the JAK-STAT pathway. This supports the hypothesis that UTI could mitigate SAE severity by inhibiting the JAK-STAT pathway, reducing *ICAM-1* expression in both the BBB and hippocampus, decreasing inflammatory mediator synthesis, and enhancing BBB stability. While *SOCS3* is known to inhibit the JAK-STAT pathway and improve sepsis outcomes,[62] evidence of UTI's regulation of *SOCS3* remains limited. Our study observed that UTI influences *SOCS3* expression in the hippocampal tissue of septic mice, though further research is required to determine whether UTI ameliorates SAE by modulating *SOCS3* to inhibit the JAK-STAT pathway. Additionally, numerous studies have shown that UTI treatment reduces inflammation and improves sepsis outcomes by downregulating *IL-1β* and *IL-6*.[77–79] Suppressing *IL-1β* and *IL-6* levels in the hippocampus of septic mice has been found to enhance spatial memory and improve survival in SAE models.[20,80] UTI treatment is also known to regulate the TLR4 signaling pathway, reducing the release of inflammatory mediators such as *IL-1β* and *IL-6*.[72,74] Our study found that UTI is associated with a reduction in the mRNA levels of *IL-1β* and *IL-6* in the hippocampal tissue of septic mice, both of which are enriched in the TLR pathway. Thus, it is plausible that UTI attenuates *IL-1β* and *IL-6* expression in the hippocampus by modulating the TLR pathway, potentially mitigating neuroinflammation and improving SAE outcomes. This study also identified enrichment of *CCL2* and *IRF7* in the TLR signaling pathway and observed reduced expression of these genes in the hippocampus of septic mice following UTI treatment. However, direct regulation of *CCL2* and *IRF7* by UTI in the context of sepsis and SAE requires further investigation. In summary, our findings suggest that UTI may improve cognitive function and reduce hippocampal damage in septic mice, indicating its potential as a therapeutic option for SAE.

It is noteworthy that UTI possesses extensive anti-inflammatory and immunomodulatory properties, which may impact SAE through the regulation of various biological processes and pathways. The dysregulation of apoptosis underlies numerous diseases.[81] Research indicates that UTI may influence the apoptotic process and exert

a neuroprotective effect by modulating the NLRP3 inflammasome[82] and the MAPK/NF-κB signaling pathways.[83] Our study identified that all six hub genes are enriched in the apoptosis pathway, indicating that UTI may modulate the apoptotic process to improve SAE by influencing the expression of these hub genes. Moreover, numerous studies indicate that the Nrf2/HO-1 pathway, linked to inflammation and oxidative stress, can be activated by UTI, offering protection against cerebral ischemia-reperfusion[84,85] and liver injuries.[86] This provides a deeper understanding of the potential mechanisms by which UTI may influence the treatment of SAE.

Additionally, significant differences were observed in the composition of infiltrating immune cells among the three groups, particularly in the decreased proportion of Treg cells in the hippocampal tissue of CLP mice compared to healthy controls. Following UTI treatment in CLP mice, a notable increase in the infiltration of Treg cells was detected. As immune suppressor cells derived from the lymphatic system, Treg cells play a pivotal role in modulating the immune response and maintaining homeostasis.[87] Research has shown that infiltrating Treg cells in the brain can effectively suppress SAE and alleviate SAE-induced psychiatric conditions by reducing neuroinflammation during the later stages of sepsis.[88] Moreover, UTI has been reported to mitigate inflammatory responses by modulating both the quantity and activity of Treg cells.[89,90] Based on these findings, UTI emerges as a potential therapeutic agent for SAE, with Treg cells likely being the key immune mediators in this treatment. However, further experimental validation is required to confirm these effects.

Drug-gene interaction analysis using the DGIdb database identified 116 potential therapeutic drugs or compounds for SAE. Among these, BINDARIT, a newly discovered compound, has demonstrated the ability to suppress glycosylation of acute-phase proteins,[91] selectively target monocytes in vivo, and reduce CCL2 production, contributing to its anti-inflammatory effects in diseases like acute pancreatitis and nephritis.[92] Studies have shown that BINDARIT can alleviate lung and liver damage in septic mice by selectively inhibiting CCL2, and it has also been shown to reduce plasma CCL2 levels in patients with sepsis,[93] making it a promising candidate for sepsis treatment. Our study also confirmed molecular docking between bindarit and CCL2, which is overexpressed in the hippocampal tissue of CLP mice. Thus, bindarit may improve SAE by selectively inhibiting CCL2 in the hippocampus, though further experimental validation is necessary. Lifitegrast, a cell adhesion inhibitor, has been shown to reduce and block leukocyte-endothelial adhesion by targeting ICAM1/ICAM3 suppression, contributing to its efficacy in various conditions.[94,95] In this study, molecular docking between lifitegrast and ICAM1 was identified, along with elevated ICAM1 expression in the hippocampal tissue of CLP mice. Further research is needed to assess the therapeutic potential of this interaction for SAE treatment.

This study has shed light on the potential molecular mechanisms and targets of UTI in treating SAE. UTI may mitigate SAE by modulating immune function through Treg cell-mediated NK cell cytotoxicity, as well as the JAK/STAT and Toll-like receptor signaling pathways, thereby reducing inflammation. However, several limitations must be acknowledged. First, our findings provide only preliminary validation of the key immune genes involved in UTI treatment of SAE in mice; additional animal and cellular experiments are needed to clarify the underlying mechanisms. Second, given the use of a sepsis mouse model, potential species-specific variations warrant further investigation with clinical samples to confirm the expression of these key genes and evaluate UTI's efficacy in treating human SAE. Furthermore, we intend to conduct experimental studies in the future focusing on NK cells, Treg cells, JAK/STAT signaling pathways, and toll-like receptor signaling pathways to enhance the robustness of our conclusions.

Conclusion

In conclusion, this study employed transcriptome sequencing and bioinformatics to identify six key immune genes (*ICAM-1, IRF7, IL-1β, CCL2, IL-6*, and *SOCS3*) associated with UTI treatment in SAE, and their expression was validated. The regulation of these genes may be influenced by pathways related to NK cell-mediated cytotoxicity, JAK/STAT signaling, and Toll-like receptor signaling, with Treg cells likely playing a pivotal role in enhancing SAE outcomes. This research represents the first investigation into the immune mechanisms potentially underlying UTI's therapeutic effects on SAE.

Data Sharing Statement

Data analyzed in this manuscript are publicly available from the Sequence Read Archive (https://dataview.ncbi.nlm.nih.gov/object/PRJNA1139345?reviewer=k5vvvke6ur8l56n8kdu643p17c).

Ethics Approval and Consent to Participate

The animal study protocol was approved by the Animal Ethics Committee of Guizhou Medical University on the Use and Care of Animals of NAME OF INSTITUTE (protocol code 2305207) for studies involving animals. This study also adhered to the ARRIVE guidelines (https://arriveguidelines.org) and Chinese Guidelines for the Care and Use of Laboratory Animals.

Author Contributions

All authors made a significant contribution to the work reported, whether that is in the conception, study design, execution, acquisition of data, analysis and interpretation, or in all these areas; took part in drafting, revising or critically reviewing the article; gave final approval of the version to be published; have agreed on the journal to which the article has been submitted; and agree to be accountable for all aspects of the work.

Funding

Disclosure

Wen Hu, Xiaoyuan Zhang, Zhen Wu, and Yushan Luo are co-first authors for this study. The authors declare that they have no competing interests in this work.

References

1. Evans L, Rhodes A, Alhazzani W, et al. Surviving sepsis campaign: international guidelines for management of sepsis and septic shock 2021. *Intensive Care Med*. 2021;47(11):1181–1247. doi:10.1007/s00134-021-06506-y
2. Zarbock A, Koyner JL, Gomez H, Pickkers P, Forni L. Sepsis-associated acute kidney injury-treatment standard. *Nephrol Dial Transplant*. 2023;39 (1):26–35. doi:10.1093/ndt/gfad142
3. Cajander S, Kox M, Scicluna BP, et al. Profiling the dysregulated immune response in sepsis: overcoming challenges to achieve the goal of precision medicine. *Lancet Respir Med*. 2024;12(4):305–322. doi:10.1016/s2213-2600(23)00330-2
4. Qin M, Gao Y, Guo S, et al. Establishment and evaluation of animal models of sepsis-associated encephalopathy. *World J Emerg Med*. 2023;14 (5):349–353. doi:10.5847/wjem.j.1920-8642.2023.088
5. Gofton TE, Young GB. Sepsis-associated encephalopathy. *Nat Rev Neurol*. 2012;8(10):557–566. doi:10.1038/nrneurol.2012.183
6. Mazeraud A, Righy C, Bouchereau E, Benghanem S, Bozza FA, Sharshar T. Septic-associated encephalopathy: a comprehensive review. *Neurotherapeutics*. 2020;17(2):392–403. doi:10.1007/s13311-020-00862-1
7. Widmann CN, Heneka MT. Long-term cerebral consequences of sepsis. *Lancet Neurol*. 2014;13(6):630–636. doi:10.1016/s1474-4422(14)70017-1
8. Brummel NE, Jackson JC, Pandharipande PP, et al. Delirium in the ICU and subsequent long-term disability among survivors of mechanical ventilation. *Crit Care Med*. 2014;42(2):369–377. doi:10.1097/CCM.0b013e3182a645bd
9. Krzyzaniak K, Krion R, Szymczyk A, Stepniewska E, Sieminski M. Exploring neuroprotective agents for sepsis-associated encephalopathy: a comprehensive review. *Int J Mol Sci*. 2023;24(13):10780. doi:10.3390/ijms241310780
10. Liu YX, Yu Y, Liu JP, et al. Neuroimmune regulation in sepsis-associated encephalopathy: the interaction between the brain and peripheral immunity. *Front Neurol*. 2022;13:892480. doi:10.3389/fneur.2022.892480
11. Ren C, Yao RQ, Zhang H, Feng YW, Yao YM. Sepsis-associated encephalopathy: a vicious cycle of immunosuppression. *J Neuroinflammation*. 2020;17(1):14. doi:10.1186/s12974-020-1701-3
12. Chen L, Jin S, Yang M, et al. Integrated single cell and bulk RNA-seq analysis revealed immunomodulatory effects of ulinastatin in sepsis: a multicenter cohort study. *Front Immunol*. 2022;13:882774. doi:10.3389/fimmu.2022.882774
13. Li T, Ji X, Liu J, et al. Ulinastatin improves renal microcirculation by protecting endothelial cells and inhibiting autophagy in a septic rat model. *Kidney Blood Press Res*. 2022;47(4):256–269. doi:10.1159/000521648
14. Cao C, Yin C, Chai Y, Jin H, Wang L, Shou S. Ulinastatin mediates suppression of regulatory T cells through TLR4/NF-κB signaling pathway in murine sepsis. *Int Immunopharmacol*. 2018;64:411–423. doi:10.1016/j.intimp.2018.09.025
15. Han D, Shang W, Wang G, et al. Ulinastatin- and thymosin α1-based immunomodulatory strategy for sepsis: a meta-analysis. *Int Immunopharmacol*. 2015;29(2):377–382. doi:10.1016/j.intimp.2015.10.026
16. Su J, Lin C, Lin X, et al. Combining ulinastatin with TIENAM improves the outcome of sepsis induced by cecal ligation and puncture in mice by reducing inflammation and regulating immune responses. *Int Immunopharmacol*. 2024;141:112927. doi:10.1016/j.intimp.2024.112927

17. Rittirsch D, Huber-Lang MS, Flierl MA, Ward PA. Immunodesign of experimental sepsis by cecal ligation and puncture. *Nat Protoc*. 2009;4 (1):31–36. doi:10.1038/nprot.2008.214

18. Zhou R, Yang X, Li X, et al. Recombinant CC16 inhibits NLRP3/caspase-1-induced pyroptosis through p38 MAPK and ERK signaling pathways in the brain of a neonatal rat model with sepsis. *J Neuroinflammation*. 2019;16(1):239. doi:10.1186/s12974-019-1651-9

19. Zhou RX, Li YY, Qu Y, et al. Regulation of hippocampal neuronal apoptosis and autophagy in mice with sepsis-associated encephalopathy by immunity-related GTPase M1. *CNS Neurosci Ther*. 2020;26(2):177–188. doi:10.1111/cns.13229

20. Jiang S, Shi D, Bai L, Niu T, Kang R, Liu Y. Inhibition of interleukin-6 trans-signaling improves survival and prevents cognitive impairment in a mouse model of sepsis. *Int Immunopharmacol*. 2023;119:110169. doi:10.1016/j.intimp.2023.110169

21. Mandić K, Milutin Gašperov N, Božinović K, et al. Integrative analysis in head and neck cancer reveals distinct role of miRNome and methylome as tumour epigenetic drivers. *Sci Rep*. 2024;14(1):9062. doi:10.1038/s41598-024-59312-z

22. Cui X, Churchill GA. Statistical tests for differential expression in cDNA microarray experiments. *Genome Biol*. 2003;4(4):210. doi:10.1186/gb-2003-4-4-210

23. Love MI, Huber W, Anders S. Moderated estimation of fold change and dispersion for RNA-seq data with DESeq2. *Genome Biol*. 2014;15(12):550. doi:10.1186/s13059-014-0550-8

24. Maag JLV. gganatogram: an R package for modular visualisation of anatograms and tissues based on ggplot2. *F1000Res*. 2018;7:1576. doi:10.12688/f1000research.16409.2

25. Gu Z, Eils R, Schlesner M. Complex heatmaps reveal patterns and correlations in multidimensional genomic data. *Bioinformatics*. 2016;32 (18):2847–2849. doi:10.1093/bioinformatics/btw313

26. Qin R, Li C, Wang X, Zhong Z, Sun C. Identification and validation of an immune-related prognostic signature and key gene in papillary thyroid carcinoma. *Cancer Cell Int*. 2021;21(1):378. doi:10.1186/s12935-021-02066-9

27. Yu G, Wang LG, Han Y, He QY. clusterProfiler: an R package for comparing biological themes among gene clusters. *Omics*. 2012;16(5):284–287. doi:10.1089/omi.2011.0118

28. Shannon P, Markiel A, Ozier O, et al. Cytoscape: a software environment for integrated models of biomolecular interaction networks. *Genome Res*. 2003;13(11):2498–2504. doi:10.1101/gr.1239303

29. Liberzon A, Birger C, Thorvaldsdóttir H, Ghandi M, Mesirov JP, Tamayo P. The molecular signatures database (MSigDB) hallmark gene set collection. *Cell Syst*. 2015;1(6):417–425. doi:10.1016/j.cels.2015.12.004

30. Miao YR, Zhang Q, Lei Q, et al. ImmuCellAI: a unique method for comprehensive T-cell subsets abundance prediction and its application in cancer immunotherapy. *Adv Sci*. 2020;7(7):1902880. doi:10.1002/advs.201902880

31. Trott O, Olson AJ. AutoDock Vina: improving the speed and accuracy of docking with a new scoring function, efficient optimization, and multithreading. *J Comput Chem*. 2010;31(2):455–461. doi:10.1002/jcc.21334

32. Zhang Z, Zhang G, Goyal H, Mo L, Hong Y. Identification of subclasses of sepsis that showed different clinical outcomes and responses to amount of fluid resuscitation: a latent profile analysis. *Crit Care*. 2018;22(1):347. doi:10.1186/s13054-018-2279-3

33. Pugia MJ, Valdes R, Jortani SA. Bikunin (urinary trypsin inhibitor): structure, biological relevance, and measurement. *Adv Clin Chem*. 2007;44:223–245. doi:10.1016/s0065-2423(07)44007-0

34. Qiu J, Xiao X, Gao X, Zhang Y. Ulinastatin protects against sepsis-induced myocardial injury by inhibiting NLRP3 inflammasome activation. *Mol Med Rep*. 2021;24(4). doi:10.3892/mmr.2021.12369

35. Saigal S, Kapoor G. Ulinastatin: is it worth using in severe sepsis? *Intensive Care Med*. 2014;40(8):1185. doi:10.1007/s00134-014-3341-5

36. Hubbard AK, Rothlein R. Intercellular adhesion molecule-1 (ICAM-1) expression and cell signaling cascades. *Free Radic Biol Med*. 2000;28 (9):1379–1386. doi:10.1016/s0891-5849(00)00223-9

37. Bui TM, Wiesolek HL, Sumagin R. ICAM-1: a master regulator of cellular responses in inflammation, injury resolution, and tumorigenesis. *J Leukoc Biol*. 2020;108(3):787–799. doi:10.1002/jlb.2mr0220-549r

38. Baby S, Reljic T, Villalba N, Kumar A, Yuan SY. Endothelial glycocalyx-associated molecules as potential serological markers for sepsis-associated encephalopathy: a systematic review and meta-analysis. *PLoS One*. 2023;18(2):e0281941. doi:10.1371/journal.pone.0281941

39. Tomasi CD, Vuolo F, Generoso J, et al. Biomarkers of delirium in a low-risk community-acquired pneumonia-induced sepsis. *Mol Neurobiol*. 2017;54(1):722–726. doi:10.1007/s12035-016-9708-6

40. Wang S, Wang B, Shi Y. Flow and ICAM1 initiate leukocyte extravasation. *Blood*. 2022;140(3):291. doi:10.1182/blood.2022017343

41. Honda K, Yanai H, Negishi H, et al. IRF-7 is the master regulator of type-I interferon-dependent immune responses. *Nature*. 2005;434: (7034):772–777. doi:10.1038/nature03464

42. Ling X, Wei S, Ling D, et al. Irf7 regulates the expression of Srg3 and ferroptosis axis aggravated sepsis-induced acute lung injury. *Cell Mol Biol Lett*. 2023;28(1):91. doi:10.1186/s11658-023-00495-0

43. Zhu Q, Wan L, Huang H, Liao Z. IL-1β, the first piece to the puzzle of sepsis-related cognitive impairment? *Front Neurosci*. 2024;18:1370406. doi:10.3389/fnins.2024.1370406

44. Hasegawa-Ishii S, Inaba M, Shimada A. Widespread time-dependent changes in tissue cytokine concentrations in brain regions during the acute phase of endotoxemia in mice. *Neurotoxicology*. 2020;76:67–74. doi:10.1016/j.neuro.2019.10.006

45. Shimada A, Hasegawa-Ishii S. Increased cytokine expression in the choroid plexus stroma and epithelium in response to endotoxin-induced systemic inflammation in mice. *Toxicol Rep*. 2021;8:520–528. doi:10.1016/j.toxrep.2021.03.002

46. Hwang YS, Jang JP, Park SH, et al. Ponciri Fructus Immaturus ethanol extract attenuates septic shock through inhibition of the STAT1 signaling pathway. *Front Nutr*. 2022;9:988309. doi:10.3389/fnut.2022.988309

47. Yu B, Chen M, Zhang Y, et al. Diagnostic and prognostic value of Interleukin-6 in emergency department sepsis patients. *Infect Drug Resist*. 2022;15:5557–5566. doi:10.2147/idr.S384351

48. Carow B, Rottenberg ME. SOCS3, a major regulator of infection and inflammation. *Front Immunol*. 2014;5:58. doi:10.3389/fimmu.2014.00058

49. Li J, Yang D, Ge S, Liu L, Huo Y, Hu Z. Identifying hub genes of sepsis-associated and hepatic encephalopathies based on bioinformatic analysis-focus on the two common encephalopathies of septic cirrhotic patients in ICU. *BMC Med Genomics*. 2024;17(1):19. doi:10.1186/s12920-023-01774-7

50. Hill A, Khalil H, Laborc K, et al. Corticosteroid treatment during sepsis alters hippocampal function in male and female survivors. *Biol Psychiatry Glob Open Sci*. 2024;4(1):336–345. doi:10.1016/j.bpsgos.2023.08.001

51. Wolff S, Klatt S, Wolff JC, et al. Endotoxin-induced gene expression differences in the brain and effects of iNOS inhibition and norepinephrine. *Intensive Care Med*. 2009;35(4):730–739. doi:10.1007/s00134-009-1394-7

52. Guha S, Paidi RK, Goswami S, Saha P, Biswas SC. ICAM-1 protects neurons against Amyloid-β and improves cognitive behaviors in 5xFAD mice by inhibiting NF-κB. *Brain Behav Immun*. 2022;100:194–210. doi:10.1016/j.bbi.2021.11.021

53. Kelly KM, Smith JA, Mezuk B. Depression and interleukin-6 signaling: a Mendelian randomization study. *Brain Behav Immun*. 2021;95:106–114. doi:10.1016/j.bbi.2021.02.019

54. Guo Y, Patil NK, Luan L, Bohannon JK, Sherwood ER. The biology of natural killer cells during sepsis. *Immunology*. 2018;153(2):190–202. doi:10.1111/imm.12854

55. Almansa R, Wain J, Tamayo E, et al. Immunological monitoring to prevent and treat sepsis. *Crit Care*. 2013;17(1):109. doi:10.1186/cc11922

56. Cai B, Cai JP, Luo YL, Chen C, Zhang S. The specific roles of JAK/STAT signaling pathway in sepsis. *Inflammation*. 2015;38(4):1599–1608. doi:10.1007/s10753-015-0135-z

57. Dietrich JB. The adhesion molecule ICAM-1 and its regulation in relation with the blood-brain barrier. *J Neuroimmunol*. 2002;128(1–2):58–68. doi:10.1016/s0165-5728(02)00114-5

58. Hofer S, Bopp C, Hoerner C, et al. Injury of the blood brain barrier and up-regulation of icam-1 in polymicrobial sepsis. *J Surg Res*. 2008;146 (2):276–281. doi:10.1016/j.jss.2007.07.021

59. Charras A, Arvaniti P, Le Dantec C, et al. JAK inhibitors and oxidative stress control. *Front Immunol*. 2019;10:2814. doi:10.3389/fimmu.2019.02814

60. Zhou Z, Zhou X, Dong Y, Li M, Xu Y. Formononetin ameliorates high glucose-induced endothelial dysfunction by inhibiting the JAK/STAT signaling pathway. *Mol Med Rep*. 2019;20(3):2893–2901. doi:10.3892/mmr.2019.10512

61. Li X, Yang Z, Chen B, Gu L, Tian G, Sui X. SOCS3 as a potential driver of lung metastasis in colon cancer patients. *Front Immunol*. 2023;14:1088542. doi:10.3389/fimmu.2023.1088542

62. Durham GA, Williams JJL, Nasim MT, Palmer TM. Targeting SOCS proteins to control JAK-STAT signalling in disease. *Trends Pharmacol Sci*. 2019;40(5):298–308. doi:10.1016/j.tips.2019.03.001

63. Clere-Jehl R, Mariotte A, Meziani F, Bahram S, Georgel P, Helms J. JAK-STAT targeting offers novel therapeutic opportunities in sepsis. *Trends Mol Med*. 2020;26(11):987–1002. doi:10.1016/j.molmed.2020.06.007

64. Duan T, Du Y, Xing C, Wang HY, Wang RF. Toll-like receptor signaling and its role in cell-mediated immunity. *Front Immunol*. 2022;13:812774. doi:10.3389/fimmu.2022.812774

65. Wang L, Lin F, Ren M, et al. The PICK1/TLR4 complex on microglia is involved in the regulation of LPS-induced sepsis-associated encephalopathy. *Int Immunopharmacol*. 2021;100:108116. doi:10.1016/j.intimp.2021.108116

66. Honda K, Yanai H, Mizutani T, et al. Role of a transductional-transcriptional processor complex involving MyD88 and IRF-7 in Toll-like receptor signaling. *Proc Natl Acad Sci U S A*. 2004;101(43):15416–15421. doi:10.1073/pnas.0406933101

67. Jia P, Xu S, Wang X, et al. Chemokine CCL2 from proximal tubular epithelial cells contributes to sepsis-induced acute kidney injury. *Am J Physiol Renal Physiol*. 2022;323(2):F107–f119. doi:10.1152/ajprenal.00037.2022

68. Buys W, Bick A, Madel RJ, et al. Substantial heterogeneity of inflammatory cytokine production and its inhibition by a triple cocktail of toll-like receptor blockers in early sepsis. *Front Immunol*. 2023;14:1277033. doi:10.3389/fimmu.2023.1277033

69. Zhou H, Coveney AP, Wu M, et al. Activation of both TLR and NOD signaling confers host innate immunity-mediated protection against microbial infection. *Front Immunol*. 2018;9:3082. doi:10.3389/fimmu.2018.03082

70. Xu K, Li H, Zhang B, et al. Integrated transcriptomics and metabolomics analysis of the hippocampus reveals altered neuroinflammation, downregulated metabolism and synapse in sepsis-associated encephalopathy. *Front Pharmacol*. 2022;13:1004745. doi:10.3389/fphar.2022.1004745

71. Zhang X, Su C, Zhao S, Li J, Yu F. Combination therapy of Ulinastatin with Thrombomodulin alleviates endotoxin (LPS) - induced liver and kidney injury via inhibiting apoptosis, oxidative stress and HMGB1/TLR4/NF-κB pathway. *Bioengineered*. 2022;13(2):2951–2970. doi:10.1080/21655979.2021.2024686

72. Wenying S, Jing H, Ying L, Hui D. The role of TLR4/MyD88/NF-κB in the protective effect of ulinastatin on the intestinal mucosal barrier in mice with sepsis. *BMC Anesthesiol*. 2023;23(1):414. doi:10.1186/s12871-023-02374-9

73. Wu J, Yan X, Jin G. Ulinastatin protects rats from sepsis-induced acute lung injury by suppressing the JAK-STAT3 pathway. *J Cell Biochem*. 2019;120(2):2554–2559. doi:10.1002/jcb.27550

74. Cao C, Yin C, Shou S, et al. Ulinastatin protects against LPS-induced acute lung injury by attenuating TLR4/NF-κB pathway activation and reducing inflammatory mediators. *Shock*. 2018;50(5):595–605. doi:10.1097/shk.0000000000001104

75. Okumura Y, Inoue H, Fujiyama Y, Bamba T. Effects of serine protease inhibitors on accumulation of polymorphonuclear leukocytes in the lung induced by acute pancreatitis in rats. *J Gastroenterol*. 1995;30(3):379–386. doi:10.1007/bf02347515

76. Di Bella D, Ferreira JPS, Silva RNO, et al. Gold nanoparticles reduce inflammation in cerebral microvessels of mice with sepsis. *J Nanobiotechnology*. 2021;19(1):52. doi:10.1186/s12951-021-00796-6

77. Li ST, Dai Q, Zhang SX, et al. Ulinastatin attenuates LPS-induced inflammation in mouse macrophage RAW264.7 cells by inhibiting the JNK/NF-κB signaling pathway and activating the PI3K/Akt/Nrf2 pathway. *Acta Pharmacol Sin*. 2018;39(8):1294–1304. doi:10.1038/aps.2017.143

78. Wang J, Zhou J, Bai S. Combination of Glutamine and Ulinastatin treatments greatly improves sepsis outcomes. *J Inflamm Res*. 2020;13:109–115. doi:10.2147/jir.S234122

79. Wang H, Liu B, Tang Y, et al. Improvement of sepsis prognosis by Ulinastatin: a systematic review and meta-analysis of randomized controlled trials. *Front Pharmacol*. 2019;10:1370. doi:10.3389/fphar.2019.01370

80. Sui DM, Xie Q, Yi WJ, et al. Resveratrol protects against sepsis-associated encephalopathy and inhibits the NLRP3/IL-1β axis in Microglia. *Mediators Inflamm*. 2016;2016:1045657. doi:10.1155/2016/1045657

81. Gortat A, Sancho M, Mondragón L, Messeguer À, Pérez-Payá E, Orzáez M. Apaf1 inhibition promotes cell recovery from apoptosis. *Protein Cell*. 2015;6(11):833–843. doi:10.1007/s13238-015-0200-2

82. Lin Y, Xu D, Gao F, Zheng X. Ulinastatin inhibits NLRP3-induced apoptosis in a PD cell model. *Ann Transl Med*. 2021;9(11):924. doi:10.21037/atm-21-1882

83. Wang L, Jiao W, Wu J, Zhang J, Tang M, Chen Y. Ulinastatin alleviates early brain injury after intracerebral hemorrhage by inhibiting necroptosis and neuroinflammation via MAPK/NF-κB signaling pathway. *Acta Cir Bras*. 2022;37(3):e370301. doi:10.1590/acb370301

84. Cui L, Cao W, Xia Y, Li X. Ulinastatin alleviates cerebral ischemia-reperfusion injury in rats by activating the Nrf-2/HO-1 signaling pathway. *Ann Transl Med*. 2020;8(18):1136. doi:10.21037/atm-20-5115

85. Wu X, Jiao W, Chen J, Tao Y, Zhang J, Wang Y. Ulinastatin alleviates early brain injury after intracerebral hemorrhage by inhibiting oxidative stress and neuroinflammation via ROS/MAPK/Nrf2 signaling pathway. *Acta Cir Bras*. 2022;37(6):e370606. doi:10.1590/acb370606

86. Wang C, Liu T, Tong Y, et al. Ulinastatin protects against Acetaminophen-induced liver injury by alleviating ferroptosis via the SIRT1/NRF2/HO-1 pathway. *Am J Transl Res*. 2021;13(6):6031–6042.

87. Ohkura N, Sakaguchi S. Transcriptional and epigenetic basis of Treg cell development and function: its genetic anomalies or variations in autoimmune diseases. *Cell Res*. 2020;30(6):465–474. doi:10.1038/s41422-020-0324-7

88. Saito M, Fujinami Y, Ono Y, et al. Infiltrated regulatory T cells and Th2 cells in the brain contribute to attenuation of sepsis-associated encephalopathy and alleviation of mental impairments in mice with polymicrobial sepsis. *Brain Behav Immun*. 2021;92:25–38. doi:10.1016/j.bbi.2020.11.010

89. Yang XY, Song J, Hou SK, et al. Ulinastatin ameliorates acute kidney injury induced by crush syndrome inflammation by modulating Th17/Treg cells. *Int Immunopharmacol*. 2020;81:106265. doi:10.1016/j.intimp.2020.106265

90. Hao X, Han J, Xing Z, et al. Urinary trypsin inhibitor attenuated inflammatory response of patients undergoing cardiopulmonary bypass by inducing activated Treg cells. *Inflammation*. 2013;36(6):1279–1285. doi:10.1007/s10753-013-9666-3

91. Zhang H, Zhi L, Moochhala S, Moore PK, Bhatia M. Hydrogen sulfide acts as an inflammatory mediator in cecal ligation and puncture-induced sepsis in mice by upregulating the production of cytokines and chemokines via NF-kappaB. *Am J Physiol Lung Cell Mol Physiol*. 2007;292(4): L960–71. doi:10.1152/ajplung.00388.2006

92. Sironi M, Guglielmotti A, Polentarutti N, et al. A small synthetic molecule capable of preferentially inhibiting the production of the CC chemokine monocyte chemotactic protein-1. *Eur Cytokine Netw*. 1999;10(3):437–442.

93. Ramnath RD, Ng SW, Guglielmotti A, Bhatia M. Role of MCP-1 in endotoxemia and sepsis. *Int Immunopharmacol*. 2008;8(6):810–818. doi:10.1016/j.intimp.2008.01.033

94. Sun H, Wang XK, Li JR, et al. Establishment and application of a high-throughput screening model for cell adhesion inhibitors. *Front Pharmacol*. 2023;14:1140163. doi:10.3389/fphar.2023.1140163

95. Shen W, Zhang X, Du R, et al. ICAM3 mediates tumor metastasis via a LFA-1-ICAM3-ERM dependent manner. *Biochim Biophys Acta Mol Basis Dis*. 2018;1864(8):2566–2578. doi:10.1016/j.bbadis.2018.05.002